

Journal of Astronomical Telescopes, Instruments, and Systems

AstronomicalTelescopes.SPIDigitalLibrary.org

ADAHELI+: exploring the fast, dynamic Sun in the x-ray, optical, and near-infrared

Francesco Berrilli
Paolo Soffitta
Marco Velli
Paolo Sabatini
Alberto Bigazzi
Ronaldo Bellazzini
Luis Ramon Bellot Rubio
Alessandro Brez
Vincenzo Carbone
Gianna Cauzzi
Fabio Cavallini
Giuseppe Consolini
Fabio Curti
Dario Del Moro
Anna Maria Di Giorgio
Ilaria Ermolli
Sergio Fabiani
Marianne Faurobert
Alex Feller
Klaus Galsgaard
Szymon Gburek
Fabio Giannattasio
Luca Giovannelli
Johann Hirzberger
Stuart M. Jefferies

Maria S. Madjarska
Fabio Manni
Alessandro Mazzoni
Fabio Muleri
Valentina Penza
Giovanni Peres
Roberto Piazzesi
Francesca Pieralli
Ermanno Pietropaolo
Valentin Martinez Pillet
Michele Pinchera
Fabio Reale
Paolo Romano
Andrea Romoli
Marco Romoli
Alda Rubini
Pawel Rudawy
Paolo Sandri
Stefano Scardigli
Gloria Spandre
Sami K. Solanki
Marco Stangalini
Antonio Vecchio
Francesca Zuccarello

SPIE.

ADAHELI+: exploring the fast, dynamic Sun in the x-ray, optical, and near-infrared

Francesco Berrilli,^a Paolo Soffitta,^b Marco Velli,^{c,d} Paolo Sabatini,^e Alberto Bigazzi,^f Ronaldo Bellazzini,^g Luis Ramon Bellot Rubio,^h Alessandro Brez,^g Vincenzo Carbone,ⁱ Gianna Cauzzi,^j Fabio Cavallini,^j Giuseppe Consolini,^b Fabio Curti,^k Dario Del Moro,^{a,*} Anna Maria Di Giorgio,^b Ilaria Ermolli,^l Sergio Fabiani,^{b,m} Marianne Faurobert,ⁿ Alex Feller,^o Klaus Galsgaard,^p Szymon Gburek,^q Fabio Giannattasio,^{a,b} Luca Giovannelli,^a Johann Hirzberger,^o Stuart M. Jefferies,^r Maria S. Madjarska,^s Fabio Manni,^t Alessandro Mazzoni,^u Fabio Muleri,^b Valentina Penza,^a Giovanni Peres,^v Roberto Piazzesi,^a Francesca Pieralli,^u Ermanno Pietropaolo,^w Valentin Martinez Pillet,^{x,y} Michele Pinchera,^g Fabio Reale,^v Paolo Romano,^z Andrea Romoli,^u Marco Romoli,^c Alda Rubini,^b Pawel Rudawy,^q Paolo Sandri,^u Stefano Scardigli,^a Gloria Spandre,^g Sami K. Solanki,^{o,aa} Marco Stangalini,^{a,l} Antonio Vecchio,ⁱ and Francesca Zuccarello^{bb}

^aUniversity of Rome “Tor Vergata”, Department of Physics, Via Della Ricerca Scientifica 1, 00133 Roma, Italy

^bINAF—Institute for Space Astrophysics and Planetology, Via del Fosso del Cavaliere 100, 00133 Roma, Italy

^cUniversity of Florence, Department of Physics and Astronomy, Via Sansone 1, 50019 Sesto Fiorentino (FI), Italy

^dUniversity of California, Los Angeles, Department of Earth, Planetary, and Space Sciences, 595 Charles Young Drive East, Los Angeles, California 90095, United States

^eOHB-CGS, Via Gallarate 150, 20151 Milano, Italy

^fSERCO S.p.A., Via Galileo Galilei 00044 Frascati (Rome), Italy

^gINFN—Pisa Section, Largo Bruno Pontecorvo 3, 56127 Pisa, Italy

^hInstituto de Astrofísica de Andalucía, Glorieta de la Astronomía, s/n, 18008 Granada, Spain

ⁱUniversity of Calabria, Department of Physics, Via P.Bucci, Cubo 31C, 87036 Arcavacata di Rende (CS), Italy

^jINAF—Arcetri Astrophysical Observatory, Largo Enrico Fermi 5, 50125 Firenze, Italy

^kUniversity of Rome “Sapienza,” Department of Aeronautical, Electrical and Energetic Engineering, Via Eudossiana 18, 00184 Roma, Italy

^lINAF—Rome Astronomical Observatory, Via Frascati 33, 00078, Monte Porzio Catone (RM), Italy

^mINFN—Trieste Section, Via Padriciano 99, 34149 Trieste, Italy

ⁿUniversité de Nice Sophia Antipolis, Avenue Valrose 28, 06103 Nice, France

^oMax Planck Institute for Solar System Research, Justus-von-Liebig-Weg 3, 37077 Göttingen, Germany

^pNiels Bohr Institute, Blegdamsvej 17, 2100 København, Denmark

^qSpace Research Centre, Polish Academy of Sciences, Bartycka 18A, 00-716 Warsaw, Poland

^rUniversity of Hawaii, Institute of Astronomy, 2680 Woodlawn Drive, Honolulu, Hawaii 96822-1839, United States

^sArmagh Observatory, Armagh BT61 9DG, Northern Ireland, United Kingdom

^tSRS-Engineering Design S.r.l., Vicolo delle Palle 25-25/B, 00186 Roma, Italy

^uANTARES s.c.a.r.l., Via Appia 1, 82018 S. Giorgio del Sannio (BN), Italy

^vUniversity of Palermo, Department of Physics and Chemistry, Viale delle Scienze, Ed. 17, 90128 Palermo, Italy

^wUniversity of L'Aquila, Department of Physics and Chemistry Sciences, Via Vetoio, 67100 Coppito (AQ), Italy

^xInstituto de Astrofísica de Canarias, C/ Vía Láctea, s/n, 38205 San Cristóbal de La Laguna, Santa Cruz de Tenerife, Spain

^yNational Solar Observatory, 3004 Telescope Loop, Sunspot, New Mexico 88349, United States

^zINAF—Catania Astronomical Observatory, Via Santa Sofia 78, Gravina di Catania (CT), Italy

^{aa}Kyung Hee University, School of Space Research, Yongin, Gyeonggi-Do 446-701, Republic of Korea

^{bb}University of Catania, Department of Physics and Astronomy, Via Santa Sofia, 64, 95123 Catania (CT), Italy

Abstract. Advanced Astronomy for Heliophysics Plus (ADAHELI+) is a project concept for a small solar and space weather mission with a budget compatible with an European Space Agency (ESA) S-class mission, including launch, and a fast development cycle. ADAHELI+ was submitted to the European Space Agency by a European-wide consortium of solar physics research institutes in response to the “Call for a small mission opportunity for a launch in 2017,” of March 9, 2012. The ADAHELI+ project builds on the heritage of the former ADAHELI mission, which had successfully completed its phase-A study under the Italian Space Agency 2007 Small Mission Programme, thus proving the soundness and feasibility of its innovative low-budget design. ADAHELI+ is a solar space mission with two main instruments: ISODY+: an imager, based on Fabry–Pérot interferometers, whose design is optimized to the acquisition of highest cadence, long-duration, multiline spectropolarimetric images in the visible/near-infrared region of the solar spectrum. XSPO: an x-ray polarimeter for solar flares in x-rays with energies in the 15 to 35 keV range. ADAHELI+ is capable of performing observations that cannot be addressed by other currently planned solar space missions, due to their limited telemetry, or by ground-based facilities, due to the problematic effect of the terrestrial atmosphere. © The Authors. Published by SPIE under a Creative Commons Attribution 3.0 Unported License. Distribution or reproduction of this work in whole or in part requires full attribution of the original publication, including its DOI. [DOI: [10.1117/1.JATIS.1.4.044006](https://doi.org/10.1117/1.JATIS.1.4.044006)]

Keywords: Sun; satellites; infrared spectroscopy; Fabry–Pérot; x-rays; polarimetry.

Paper 15065 received Jul. 27, 2015; accepted for publication Nov. 6, 2015; published online Dec. 11, 2015.

*Address all correspondence to: Dario Del Moro, E-mail: delmoro@roma2.infn.it

1 Introduction

The understanding of solar magnetic field generation and evolution is one of the most outstanding problems in solar and stellar physics.

The solar magnetic field is continuously generated and destroyed on timescales ranging from fractions of a second to years, and fills the heliosphere, a volume of space that extends to at least 10×10^9 km from the Sun. Also, the solar magnetic field drives solar activity on all timescales from second to centuries, abruptly enhancing the emission of particles and x-ray from our star, but also leading to gradual long-term changes in its radiative output. Consequently, these processes dictate space weather, and how the solar plasma, radiation, and magnetic field interact with planetary environments; changes in the magnetic field drive solar activity and eventually define the space weather conditions. Solar activity forecasting is therefore a major issue of ESA Space Situational Awareness activities for the security of space assets. In addition, an investigation of the structure and dynamics of the magnetic field in the photosphere and in the chromosphere are fundamental to solve the mystery of the Sun's superhot corona or resolving fundamental problems in solar physics, such as the origin and acceleration of the fast solar wind.

Advanced Astronomy for Heliophysics Plus (ADAHELI+) is the first and only solar space mission specifically designed to provide: (i) multiline spectropolarimetric imaging at high cadence (5 fps) and exceptionally long-duration observations of target regions in the photosphere and chromosphere; (ii) x-ray polarimetry of solar flares in the 15- to 35-keV energy. ADAHELI+ is capable of performing observations that cannot be addressed by other currently planned solar space missions, due to their limited telemetry, or by ground-based facilities, due to the problematic effect of the terrestrial atmosphere.

ADAHELI+ is a solar space mission with two main instruments:

- ISODY+: an imager whose design is optimized to the acquisition of the highest cadence, long-duration, multiline spectropolarimetric images in the visible/near-infrared (VIS–NIR) region of the solar spectrum.
- XSPO: an x-ray polarimeter which will, for the first time, perform polarimetry of solar flares in x-rays (15 to 35 keV).

ADAHELI+ builds on the heritage of the ADAHELI mission^{1–6} and the expertise of its industrial team with building and operating a small satellite mission. ADAHELI successfully completed its phase-A study under the Italian Space Agency (ASI) 2007 Small Mission Programme, proving the feasibility of its innovative low-budget design. ADAHELI+ was one of the 26 proposals submitted to the European Space Agency in response to the call for a small mission ESA D/SRE/FF/og-28226 issued on March 9, 2012, but was not selected.

2 Key Technologies and Design Solutions

ADAHELI+ has been designed to match the requirements of its high-performance VIS–NIR telescope, a diffraction-limited 500-mm Gregorian solar telescope of 0.25 arc sec angular resolution (corresponding to 175 km on the Sun), capable of acquiring a quasisimultaneous series of fully two-dimensional (2-D) spectral images of the solar lower atmosphere at a rate of up to 5 frames/s, to reconstruct the three-dimensional (3-D) structure of the Sun's magnetic fields.

A number of innovative solutions have been devised in order to meet the requirements within the limits of a small mission. The fast imaging and spectral scanning capability is made possible by the use of a Fabry–Pérot interferometer (FPI), flying for the first time in this class of satellites.

FPIs have a much higher transmittance (by a factor 30) with respect to long slit spectrograph of the same spectral resolution.⁷ FPI-based instruments are capable of acquiring a 2-D image at high spectral resolving power (better than 200,000, and have a very fast wavelength tuning, of the order of tens of milliseconds, resulting in the possibility of building stacks of 2-D tomographic images. FPIs have been selected, for their high performances, to be used in future large missions such as the James Webb Space Telescope, BepiColombo, and Solar Orbiter.^{8–10} A wide operational spectral range is achieved due to the capacitance-stabilized piezoelectric control of the FPI¹¹ (which is, in that case, often referred to as CSE–FPI: capacitance-stabilized etalon–FPI) and suitable cameras.

A great effort has been dedicated to redesign the ISODY+ layout, with respect to that of its precursor ISODY,^{3,4} to adopt an all-reflective design, minimizing both aberrations and mechanical complexity.

The high resolution of the telescope needs high-precision tracking of the region of interest (ROI), to less than 0.1 arc sec during the acquisition. This is achieved by the combined action of the satellite attitude and orbit control system (AOCS) and the correlation tracker (CRT) correction system in ISODY+.

For the thermal control of the VIS–NIR telescope, particular attention has been given to ensure a drastic reduction of the heat power reflected from the primary mirror. A dedicated heat rejecter has therefore been designed.

X-ray solar polarimeter (XSPO) exploits the capability of the gas pixel detector (GPD)^{12,13} to reconstruct the emission direction of the photons absorbed via photoelectric effect in gas to derive the polarization of detected radiation. Also, a Peltier cooler takes care of keeping the GPD operative temperature in the required [5 to 20°C] range, with optimal working temperature of 10°C and a stability of $\pm 2^\circ\text{C}$.

A compact design has been adopted with the payload and the platform integrated in the same structure. All the internal units are then accommodated around the main telescope.

In order to address the launch costs, the overall satellite envelope has been designed to be compatible with a dual launch through the ESA small launcher VEGA.

The ground segment has been designed to cost and makes use of the ASI Acquisition Station and Satellite Control Center in Matera and Fucino (Italy), respectively. These stations are located at midlatitudes and the visibility time of the ground stations to the satellite is about 50 min/day. However, the constraints in attitude pointing during observations, imposed by the telescope, and the intrinsically limited coverage of an X-band antenna, reduce the available time for data download to 25 min/day. This requires a high data rate in downlink, of at least 150 Mbps, achieved by a special development of the X-band antenna.

Science operations are managed by science personnel for long-term payload operations planning, quick-look analysis, processing, data distribution, and quality assessment.

Processing and archiving infrastructures are hosted and managed through the ASI Scientific Data Center.

3 Science Goals

Understanding our own star is one of the major scientific challenges recognized by all space programs, see, e.g., NASA's

Living with a Star Program and ESA's Cosmic Vision 2015 to 2025. ADAHELI+ is designed to specifically target a set of fundamental questions in heliophysics:

- What determines the Sun's superhot corona?
 - How does the magnetic field couple the solar atmosphere from the photosphere to the high chromosphere?
 - What is the role of waves in the Sun's corona?
- How is the magnetic field generated and destroyed on timescales ranging from fractions of a second to years?
 - What is the nature of the coupling of magnetic field and photospheric plasma, in particular, in the polar regions?
- What is the nature of the polarization of hard x-ray (HXR) sources in the solar atmosphere?
 - How is the fast solar wind generated and accelerated?

3.1 Heating the Corona: Chromospheric Fields and Dynamics

3.1.1 Chromosphere fast dynamics

The chromosphere is the “interface layer” between the photospheric plasma dominated by turbulent convective motions, and the tenuous corona where most of the structure is determined by the magnetic field. This atmospheric region still presents crucial observational and theoretical challenges. In the chromosphere, compressible waves excited at the photospheric roots of the granular convection, or through p-mode conversion, steepen and form shocks, accounting for large dynamical excursions and very short timescales, of a few minutes at most,^{14–16} requiring a fully time-dependent analysis. Understanding the mechanisms that sustain the chromosphere departure from radiative equilibrium will pave the way to understanding the formation of the super-hot corona and the origin of the solar wind. ADAHELI+ provides high-rate, long-duration observations to cover a large interval in the VIS–NIR range. Table 1 reports the observational requirements related to the study of the dynamics of the chromosphere.

3.1.2 Waves and heating of the solar upper atmosphere

The temperature at the top of the Sun's chromosphere (~10,000 K) is higher than at the bottom (~4300 K). Different mechanisms have been proposed to explain this rise in temperature, from the dissipation of upward-propagating waves,¹⁷ to resistive dissipation of fine-scale electric currents,¹⁸ to magnetic field reconnection.¹⁹ These waves, usually considered evanescent in a nonmagnetic atmosphere, propagate through so-called magnetoacoustic portals that are generated where the magnetic field is significantly inclined. Such conditions are ubiquitous on the Sun, both in active regions (ARs) and at the boundaries of convection cells.²⁰ In addition to these, magneto-hydrodynamic (MHD) waves in magnetic structures can also significantly participate in the energy budget of the upper layers of the Sun's atmosphere. In particular, small-scale magnetic elements cover a significant fraction of the solar photosphere^{21,22} and harbor different kinds of waves that connect different layers of the

Table 1 Chromosphere fast dynamics: observational requirements.

Objective	Chromospheric and photospheric vector magnetic field and line of sight velocity field maps, large FOV, long-duration
Method	Simultaneous sampling of photospheric and chromospheric lines
Spectral lines	HeI 1083.0 nm line (chromosphere) SiII 1082.7 nm line (photosphere) CaII 854.2 nm line (chromosphere) FeI 617.3 nm line (photosphere)
FOV	100 arc sec × 100 arc sec to properly encompass the extent of a typical AR
Spatial resolution	0.5 arc sec at 1 μ m
Spectral resolving power	150,000
Photometry	10 ⁸ photons
Polarimetric precision	S/N 10 ⁴
Data set duration	>2 h
Full spectral scan cadence	<1 min

solar atmosphere, eventually depositing a significant amount of energy in the upper chromosphere (see, e.g., Refs. 23 and 24 for a complete treatment of the topic). Among the many different kinds of MHD waves that small flux tubes can support (compressive and noncompressive), kink waves are probably the most promising due to their ability to travel long distances before being dissipated.^{15,16,25,26} Very recently, observations have revealed the propagation of kink waves in small magnetic elements to the solar chromosphere, with velocity of the order of 6 km/s.²⁷ However, although these authors have shown that this propagation is highly nonlinear, and thus subject to dissipation, no signature of energy losses was found between the photosphere and the chromosphere. For these reasons, a new fundamental question arises as to which are the main mechanisms responsible for the dissipation of the energy contained in MHD waves and operating at different heights of the solar atmosphere. To this regard, multi-height high spatial resolution spectropolarimetric observations are needed to study in detail the propagation mechanisms of different kinds of MHD waves and to assess the main dissipation mechanisms involved. Table 2 reports the observational requirements set by the investigation of waves in the solar atmosphere.

3.2 Magnetic Flux Emergence, the Solar Wind, and the Dynamo

3.2.1 Prominences, reconnection, and magnetic flux emergence; origin and acceleration of the fast solar wind

Prominences are chromospheric features rooted in the photosphere and extending out of either sides of a primary spine. Magnetic reconnection may create plasma upflows in filaments:

Table 2 Waves in the solar atmosphere: observational requirements.

Objective	Multiheight vector magnetic field and line of sight velocity field maps
Method	Simultaneous full-Stokes sampling of photospheric and chromospheric lines
Spectral lines	HeI 1083.0 nm line (chromosphere)
	SiI 1082.7 nm line (photosphere)
	CaII 854.2 nm line (chromosphere)
	Fel 617.3 nm line (photosphere)
Data set duration	>30 min
Full scan cadence	10 to 30 s

as reconnection proceeds, the lower reconnected loops submerge below the solar surface, while the upper ones move upward and carry photospheric plasma with them. Presently, chromospheric jet-like events such as spicules/mottles (in the quiet Sun)^{28,29} and fibrils (in ARs)³⁰ are investigated both through the latest generation of ground-based instruments,^{31,32} together with the space-based observatories Hinode and Solar Dynamics Observatory.^{33,34} Hinode observations of high-velocity spicules have recently revived the discussion on the contribution of these phenomena to coronal heating and solar wind generation.^{32,34} However, the short observation times typically allocated to this type of observations on space observatories, due to the shared telemetry among different instruments, and the intrinsic limitations of ground-based observations, hamper further advances on this subject. Experimental confirmation of magnetic reconnection models requires high cadence observations of photospheric and chromospheric lines searching for cancellation of magnetic flux and plasma motions along the line of sight. Uninterrupted space observations with long-time surveys of coronal holes in equatorial and polar regions, available through a dedicated mission such as ADAHELI+, will advance our understanding of where and how the fast solar wind is generated and accelerated.³⁵ Table 3 reports the observational requirements associated with the analysis of chromospheric features.

3.2.2 Magnetic flux emergence and quiet Sun magnetism

Magnetic flux emergence is a complex process involving a wide range of time and spatial scales: from the large ARs present during solar maxima (with flux content up to 10^{23} Mx) that host the most violent phenomena associated with energy release (flares, eruptive prominences, CMEs), to small bipolar flux concentrations (ephemeral regions and granular bipoles, with fluxes from 10^{16} to 10^{19} Mx), which populate the quiet Sun at all times during the solar cycle. Recent observations of the solar magnetic surface with space- and ground-based instruments have shown how the quiet Sun magnetic fields can no longer be regarded as sheets of unipolar magnetic flux stretching along the boundaries of large convection cells (i.e., supergranules). Ubiquitous transverse magnetic fields (see, e.g., Refs. 36–38) and fine intranet-work mixed polarity fields (see, e.g., Refs. 39 and 40) have been discovered using Hinode instruments.⁴¹ Moreover, the launch of the IMAx spectropolarimeter⁴² on-board the Sunrise balloon-borne solar observatory,^{43,44} allowed the resolution of individual

Table 3 Prominences: observational requirements.

Objective	Vector magnetic field maps, plasma motions in barbs, localization of plasma motions, and brightenings as signatures of magnetic reconnection, large FOV, long-duration
Method	Simultaneous full-Stokes sampling of photospheric and chromospheric lines
Spectral lines	HeI 1083.0 nm line (chromosphere)
	SiI 1082.7 nm line (photosphere)
	CaII 854.2 nm line (chromosphere)
	Fel 617.3 nm line (photosphere)
FOV	100 arc sec × 100 arc sec
Spatial resolution	0.5 arc sec
Spectral resolving power	150,000
Data set duration	>2 h
Full scan cadence	10 s

kilo-Gauss fluxes⁴⁵ and the exploration of vortex flow motions.⁴⁶ This new information suggests that the quiet Sun magnetic fields are not magnetic debris from decaying ARs but have rather to be generated through some other small-scale mechanisms.⁴⁷ Large fields of view [(FOV) supergranular scale], time-extended observations (>24 h), high spatial resolution, and fast time cadence are needed to investigate long-lived structures and see how the intermittent magnetic field appears and disappears. Table 4 reports the observational requirements set by the investigation of quiet Sun magnetism.

3.3 Solar Flares

3.3.1 X-ray polarimetry of solar flares

Due to energetic events such as solar flares, the Sun is an astrophysical source with an intense emission of x-rays. Their characterization will advance our understanding of the dynamics of the magnetic fields in the ARs of our star. Magnetic reconnection is the cause of the sudden release of energy in flares and it is responsible for the acceleration of particles,^{48–50} including the downward beaming and the upward solar wind. The nonthermal HXR emission, dominating at energies ≥ 15 keV, is generated by electrons slowing-down in the plasma of the solar atmosphere. Particles radiate via bremsstrahlung and heat the ambient plasma. This emission component is expected to be highly polarized,^{51–56} with a polarization degree as high as 40% at 20 keV.⁵⁷ Polarization measurements are directly correlated to the study of the particles' acceleration directivity and therefore to the understanding of the plasma environment. There have been recent attempts to measure the x-ray polarization with the RHESSI satellite and with the Thomson-scattering polarimeter SPR-N on board of the CORONAS-F satellite.^{58–60} Both instruments had a small effective area for polarization measurements and were also heavily affected by the background. Furthermore, the RHESSI spectrometer (not specifically designed to operate as a polarimeter⁶¹) has a high energy threshold

Table 4 Quiet Sun magnetism: observational requirements.

Objective	Vector magnetic field maps, small magnetic elements polarimetric observation, plasma motions in emerging and submerging regions, localization of brightenings, large FOV, very long-duration
Method	Full-Stokes sampling of photospheric lines
Spectral lines	SiI 1082.7 nm line (photosphere) FeI 617.3 nm line (photosphere)
FOV	100 arc sec×100 arc sec to encompass several supergranular structures
Spatial resolution	0.5 arc sec
Spectral resolving power	110,000
Data set duration	≈24 h
Full scan cadence	5 s

for polarimetric measurements (100 keV), thus encountering the problem of the fast decrease of the x-ray flare flux. Neither instruments, therefore, reached the sensitivity needed to achieve significant results. Future missions, e.g., solar orbiter, will not address x-ray polarimetry among their science topics. The photoelectric polarimeter XSPO on board ADAHELI+ is a unique opportunity to complement all the other efforts for the understanding of solar flares. This instrument will perform sensitive x-ray polarimetry in the 15- to 35-keV energy band, in a spectral region where the highly polarized HXR emission starts to overwhelm the SXR component. Additional science topics related to fundamental physics can be addressed with the XSPO: a long-term accumulation of angular resolved data is suitable to reveal the presence of an x-ray-emitting region from the solar disc center, produced by the interaction of axions particles with local magnetic field and also the ARs may prove a good probe for searching for the axionic x-rays.^{62,63} Table 5 reports the observational requirements set by the investigation of X-ray polarimetry of solar flares.

4 Observation Goals and Strategy

4.1 VIS–NIR Polarimetry for Chromospheric and Photospheric Diagnostic

The best diagnostics for chromospheric polarimetry lie in the NIR range. Science mission goals, as set in Sec. 3, will be

Table 5 X-ray polarimetry of solar flares: observational requirements.

Objective	Particle acceleration and plasma conditions during flares
Method	Polarization measure of x-rays
Energy band	15 to 35 keV
FOV	70 arc min (fully coded)
Angular resolution	1 arc min

Table 6 VIS-NIR telescope main characteristics.

Characteristic	Value
Wavelength range	From 400 to 1100 nm
FOV	108 × 108 arc sec
M1 mirror diameter	500 mm
Mirror type	Concave prolate ellipsoid (almost parabolic)
M2 mirror diameter	164 mm
Mirror type	Concave prolate ellipsoid
M1–M2 distance	1152 mm
EFL telescope	3465 mm
Entrance pupil	500 mm
Obscuration	172 mm
Exit pupil	30 mm
Resolution	Diffraction limited

achieved through observations of quasisimultaneous chromospheric (CaII 854.2 nm or HeI triplet 1083 nm) lines, producing maps of intensity, full magnetic vector, and Doppler velocity. Both lines are sensitive to Hanle and Zeeman effects, making them unique diagnostic tools for chromospheric magnetic fields covering a wide range of strengths. While the detailed physics of formation is complicated by many factors, spectral line inversion codes to analyze the emergent spectral line radiation in a variety of physical scenarios do exist and are becoming available to the scientific community (see, e.g., Refs. 64–67). In particular, observations and theory show that the HeI triplet is better suited for ARs studies, while the CaII line is to be employed for quieter conditions, and for cross-calibration with ground-based instrumentation.

Moreover, a photospheric, magnetically sensitive line (SiI 1082.7 nm), is available in the immediate spectral surroundings of the He triplet: this is crucial in order to obtain quasisimultaneous maps of photospheric magnetic fields that will aid the

Table 7 ISODY+ narrowband channel parameters.

Characteristic	Value
Spectral lines	HeI triplet at 1083 nm CaII line at 854.2 nm FeI line at 617.3 nm SiI line at 1082.7 nm
Spectral resolving power	$\delta\lambda/\lambda > 150,000$
Wavelength stability	Maximum drift 10 m/s in 10 h
Polarimetric accuracy	10^2 to 10^4

interpretation of the polarimetric data in the chromosphere and the extrapolation to higher atmospheric levels. Finally, the much used and relatively well-known Fe I 617.3 nm line can be used for photospheric diagnostic purposes (e.g., magnetic field, temperature, and line of sight velocity) as well as for cross-calibration with ground-based instrumentation.

Similarly to ADAHELI+, Hinode “was designed to address the fundamental question of how magnetic fields interact with the ionized atmosphere”⁶⁸ and is the modern touchstone for high-resolution solar observation from space. The Solar Optical Telescope (SOT) onboard the spacecraft is designed to perform high-accuracy polarization measures and the design of ISODY+ builds on the lessons learnt from SOT-Narrowband Filter Instrument (NFI), trying to avoid the problems at launch encountered by its Lyot filters. On top of that, ISODY+ follows the same extremely successful observatory style mission as Hinode, with the aim to continue the high-resolution observation of the vector magnetic field in the solar atmosphere.

ADAHELI+ also shares some scientific goals with the interface region imaging spectrograph (IRIS) mission.⁶⁹ In particular, both missions want to investigate the mechanism of the coronal heating, through the analysis of MHD waves propagation and studying the dynamics of the chromosphere and the nonthermal processes that heat the solar atmosphere.⁷⁰

Although based on a different approach (FPI versus long-slit spectrography), ISODY+ and the IRIS far-UV and near-UV instruments have comparable performances. IRIS has an FOV slightly wider (175 arc sec⁶⁹), same spatial resolution, and a similar temporal resolution compared to the spectroscopic mode of ISODY. Nevertheless, ADAHELI+ can do spectropolarimetry and has a spectral resolving power ~ 3 times higher than IRIS. IRIS is devoted to explore the higher layers of the solar atmosphere, with four diagnostic lines from the photosphere to the transition region and has possibility to explore the hottest layers of the corona with a lower time resolution, while ADAHELI+ is more performing in the photospheric and chromospheric regions.

4.2 Observation Strategy

Science requirements demand quasisimultaneous measures of chromospheric (Ca II 854.2 nm or He I triplet 1083 nm) and photospheric (Fe I 617.3 nm or Si I 1082.7 nm) intensity, magnetic field components, and Doppler velocity to generate:

- line-of-sight Doppler velocity 3-D maps,
- high cadence phase maps of propagating waves and plasma jets,
- Full-Stokes spectropolarimetric data-cubes, and
- long-period spectroscopic observations.

The duration of the observations will exceed 4 h each day of operations, with the capability of performing a 24 h acquisition every month. Four standard observation modes have been devised to produce the previously mentioned data-products:

1. fast spectroscopy mode: 2 lines scan of Stokes I with 6 points each;
2. standard spectroscopy mode: 2 lines scan of Stokes I with 23 points each;
3. fast spectropolarimetry mode: 2 lines scan of Stokes I, Q, U, V with 6 points each;
4. standard spectropolarimetry mode: 2 lines scan of Stokes I, Q, U, V with 23 points each.

4.3 Line Sampling Strategy

Figure 1 shows the sampling strategy for Fe 617.3 nm and Ca 854.2 nm lines for the standard spectropolarimetric mode. The estimate of the double FPI passband is based on the IBIS^{72–74} passband shape. In the case of an acquisition rate of 5 fps, 100 ms of integration time and 1.5 s to change from a spectral region to the other, the spectral scans of 2 lines will take: (a) 4 s,

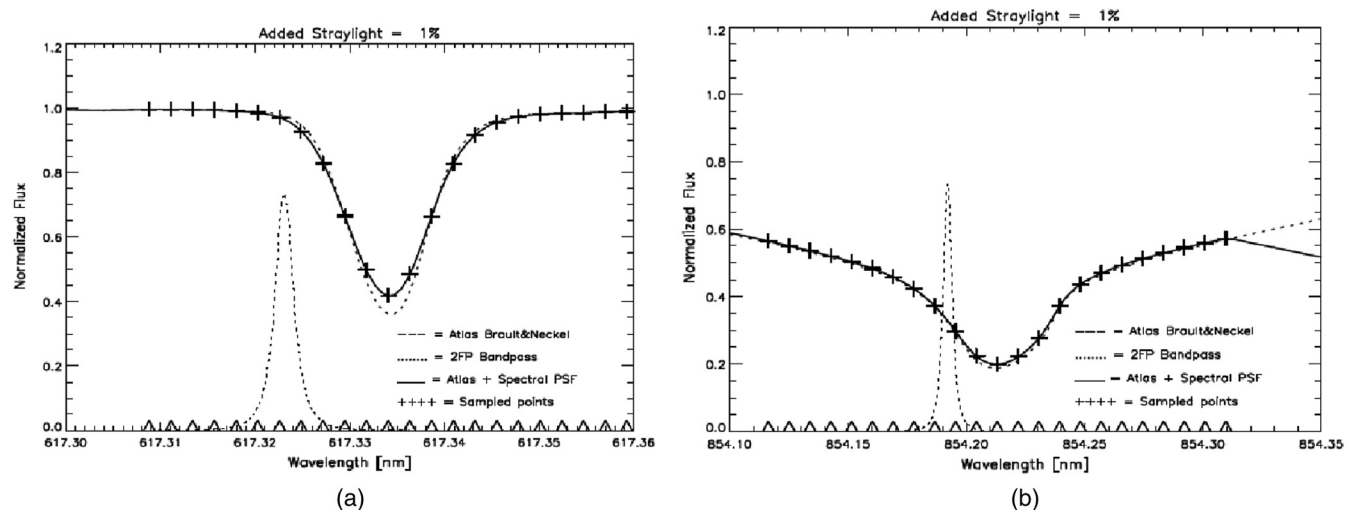


Fig. 1 Sampling points for (a) Fe 617.3 nm and (b) Ca 854.2 nm lines in the case of standard spectropolarimetric mode. Proposed sampling wavelengths are represented as triangles on the wavelength axis. The dashed line is the observed solar disk-center Fourier transform spectrometer spectrum.⁷¹ The solid line is the measured solar spectrum considering ISODY+ passband and a 1% of stray light contribution. The crosses mark the expected measures by the standard spectropolarimetric mode. ISODY+ passband (dotted line) has been estimated from the IBIS⁷² passband shape.

(b) 11 s, (c) 17 s, and (d) 60 s, respectively, for the 4 standard acquisition modes. This integration time allows a spectropolarimetric accuracy of 10^2 . Polarimetric accuracy of 10^3 or 10^4 can be traded with temporal resolution extending accordingly the integration time. Table 7 summarizes ISODY+ observation parameters.

5 ADAHELI+ Payload

5.1 ISODY+: the VIS–NIR Telescope

Interferometer for Solar Dynamics Plus (ISODY+) is a Gregorian telescope interfaced with three main instruments: a narrowband spectropolarimeter, based on FPIs, a broadband imager for high spatial resolution, and a CRT used as an image stabilization system.

5.1.1 Gregorian Telescope

The telescope relies on a classic Gregorian 2 mirrors layout (see Fig. 2), with an intermediate primary focus allocating a tilted and drilled mirror (FM1), whose function is to reject the radiation outside of the FOV. The elliptic hole of this mirror acts as field stop. FM1 is located in the shadow of M2. A second field stop (FS2) is located behind M2. It stops the light coming directly from the entrance pupil and entering the instrument. A collimator unit (CU) images at infinity the telescope focal plane. Auxiliary components are allocated before the instruments:

- The CU images at infinity the telescope focal plane and reduces the pupil diameter to 30 mm. The exit pupil diameter is a good compromise between the clear aperture of the FPIs and the incidence angle on them. The collimator is a spherical mirror (SM in Fig. 3) positioned off-axis.
- The polarization modulation unit (Fig. 3) is located after SM in parallel beam, and the sensitivity to polarization introduced by SM has been evaluated. The difference of reflectivity between P and S polarizations is 2×10^{-4} at maximum.

- The tip tilt mirror (TTM) is operated by piezoactuators driven by the CRT and it allows us to recover pointing errors caused by vibrations and thermal distortions of the structure.

Table 6 reports the main characteristics of the telescope.

The telescope effective focal length has been chosen as a trade-off between the overall volume, the relief of the instrumental box, and the accommodation inside of focal plane suite.

5.1.2 Focal plane instruments

The focal plane suite consists of a correlation tracker channel (CRTC), the broadband channel (BBC), and the narrowband channel (NBC). The three channels are arranged in order to optimize the space inside the instrumental box ($600 \times 600 \times 300 \text{ mm}^3$), located behind the telescope. The channels have been developed taking advantage of a 3-D disposition (see Fig. 3). After the TTM, a suitable dichroic mirror splits the NBC from the BBC. The NBC is able to discriminate very narrow wavebands ($3.8 \text{ pm} \pm 0.5 \text{ pm}$ at 810 nm) and retrieve information on the polarization state of the selected photospheric and chromospheric VIS–NIR lines. This is accomplished by using 2 tunable CSE–FPI and a filter wheel (not shown in Fig. 3). The FPIs combine high-spectral resolution with short exposure times and a large FOV, as well as the ability to work in polarized light. After the FPIs, the first corrector plate (CP1) reflects the beam toward the second one (CP2). The aspherical mirror (CM) focuses on CMOS1 the beam after the folding mirror (FM2).

In the BBC, the mirror (FM1) folds the beam toward 2 corrector plates (CP1 and CP2, same as in NBC). Then a beam splitter (BS) divides the incoming light between the proper BBC and the CRTC. The BBC is focused by an aspherical mirror (CM) and a folding mirror (arranged as for the NBC) on CMOS2, with a filter wheel located between BS and CM.

The CRTC is a specular copy of the BBC, with a single interference filter in the place of the filter wheel, whose image is focused on CMOS3.

The main parameters of ISODY+ are summarized in Table 8. Further details on the BBC and the CRTC are given in Refs. 2 and 75.

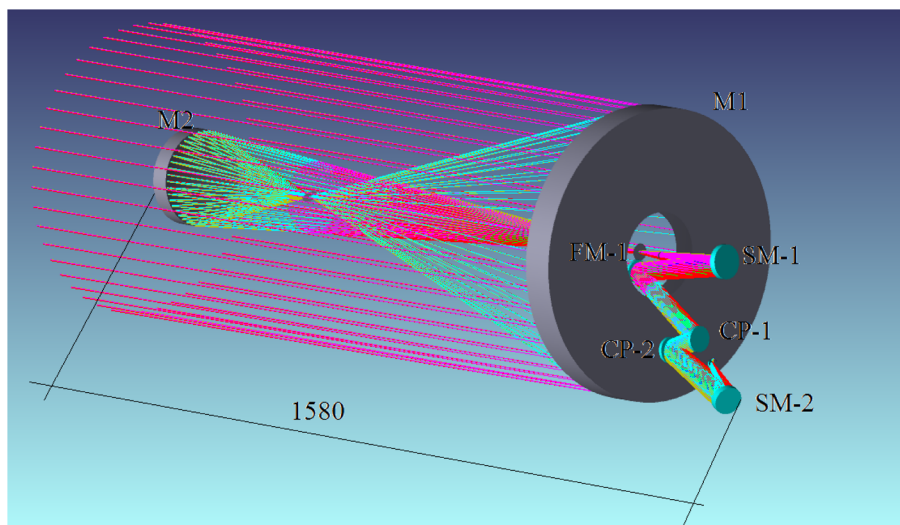


Fig. 2 Optical layout of the 50-cm Gregory telescope of ISODY+. M1, main mirror; M2, secondary mirror; FM1, folding mirror; SM1, first spherical collimating mirror; CP1, first correcting plate; CP2, second correcting plate; and SM2, aspherical mirror. Overall instrument length is 1580 mm.

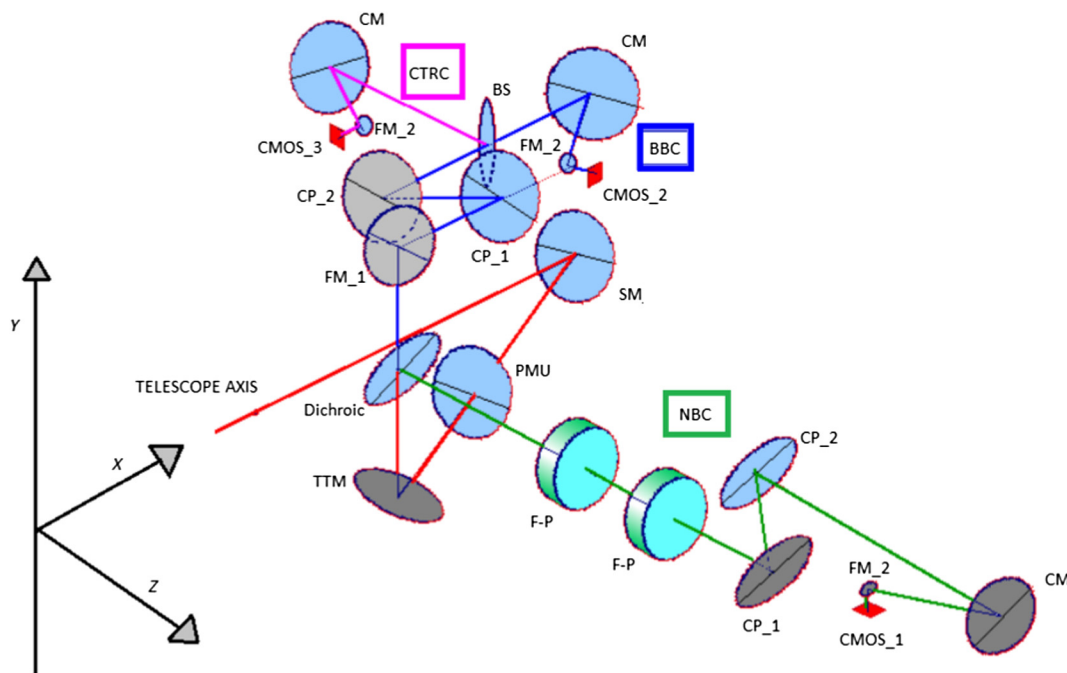


Fig. 3 ISODY+ focal plane layout. The focal plane suite consists of a correlation tracker channel (CTRC), the broadband channel (BBC), and the narrowband channel (NBC). SM, spherical mirror; PMU, polarization modulation unit; TTM, tip-tilt mirror; dichroic, dichroic mirror to split the NBC from the BBC; F-P, CSE-FPI; CP1 and CP2, corrector plates; CM, aspherical mirror; FM1 and FM2, folding mirrors; CMOS1, NBC CMOS sensor; BS, beam splitter; CMOS2, BBC CMOS sensor; and CMOS3, CTRC CMOS sensor.

5.2 XSPO: the X-Ray Instrument

5.2.1 Gas pixel detector

The GPD is a gas-filled detector devoted to study the polarization of x-ray radiation,^{12,13} and it was developed by the Pisa INFN section in collaboration with the INAF-Institute for Space Astrophysics and Planetology. It exploits the dependence of the photoelectric cross section to the polarization of photons to perform the polarimetric measurement. For each x-ray photon absorbed in the gas cell, a photoelectron is emitted with higher probability along the photon polarization direction. The ionization track is drifted and amplified by the gas electron multiplier and eventually collected on a fine subdivided pixel plane (50 μm of pitch). The detector has an active area of $1.5 \times 1.5 \text{ cm}^2$ and has self-trigger capability that allows for downloading the collected charge only from the small pixel region interested by a track. In Fig. 4 a photoelectron track imaged by the GPD is shown. The analysis of the statistical momenta of the charge distribution allows for calculating the position, projected on

the pixel plane, of the absorption point (opposite to the Bragg peak at the end of the track, where a photoelectron loses the largest fraction of its energy) and of the emission direction. In more detail, the image of the track, obtained by means of charge collection of each nonzero pixel of the ASIC subframe, allows for determining the impact point and the emission direction, which is correlated to the polarization of the incoming beam. First, it is calculated the barycenter and the angle that

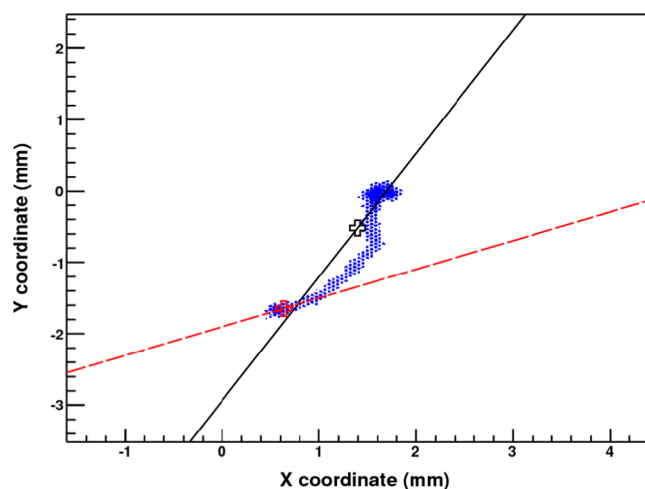


Fig. 4 Example of a photoelectron track produced by the absorption of a photon at 22 keV acquired with the GPD filled with an Ar (70%)–DME (30%) gas mixture at the pressure of 2 bar. The upper black cross is the barycenter of the charge distribution and the black solid line is the main axis of the track. The lower red cross is the absorption point and the red dashed line is the emission direction of the photoelectron.

Table 8 Main parameters on ISODY+ and XSPO instruments.

Instrument	ISODY+	XSPO
Size	$600 \times 600 \times 300 \text{ mm}^3$	$140 \times 200 \times 1000 \text{ mm}^3$
Mass	$\approx 30 \text{ kg}$	$\approx 29 \text{ kg}$
Power	$< 100 \text{ W}$	$\approx 30 \text{ W}$
Optical layout	Completely reflective	Coded-mask aperture
Detector type	CMOS sensor	GPD sensor

Table 9 Technology readiness level—platform.

Subsystem/unit	TRL	Remarks
OBDH	9	Unit based on flight proven HW and SW
PEB	9	Unit based on flight proven HW
Solar array	9	Fixed solar panels with triple junction GaAs cells
Li-ion battery	9	Based on modular design. Already flown on AGILE and LARES, under procurement for PRISMA mission
TM/TC (S-band)	9	Commercial off-the-shelf equipment
S-band antenna	9	Commercial off-the-shelf equipment
Reaction wheel	9	Commercial off-the-shelf equipment
Magnetic torquer	9	Commercial off-the-shelf equipment
Magnetometer	9	Commercial off-the-shelf equipment
Star sensor	9	Commercial off-the-shelf equipment
Gyro box	9	Customization of commercial off-the-shelf equipment. Qualified for PRISMA mission
GPS	9	Commercial off-the-shelf equipment
Structure and mechanism	9	Modular design based on flight proven structural elements. No mechanisms on platform (i.e., fixed solar array and no deployable elements on board)
Thermal S/S	9	Design based on passive control and flight proven elements

maximizes the second moment with respect to the barycenter (main axis) using all the nonzero pixels. Second, using the sign of the third moment, it is identified which part of the track contains the absorption point which has less charge density with respect to the Bragg peak (end of the track). At this point, the algorithm identifies a region in the initial part of the track using the second moment as a weight, and it evaluates again the barycenter of this part (impact point) and the angle that maximizes the second moment with respect to impact point. This is the retrieved emission direction and its distribution in angle (modulation curve) is related to the polarization of the photon beam,^{13,76} which is measured by a \cos^2 fit to the modulation curve. In the example reported in Fig. 4, the black cross and the continuous black line are the barycenter of the distribution of the charges generated in the GPD by a 22 keV and the main axis of the track, respectively. This information is used to compute the absorption point of the electron on the GPD (marked by a red cross) and the corresponding photoelectron emission direction (drawn as a dashed red line).

The GPD is, therefore, an instrument capable of performing polarimetric measurements, while acquiring the image of the source, and it has also a moderate spectroscopic capability with an energy resolution of about 20% at 5.9 keV.

The Ar-based gas mixture considered for the ADAHELI+ mission [Ar (60%)–DME (40%) at 3 bar] is suitable to measure the x-ray polarization in the 6- to 35-keV energy range.^{77,78} To allow a high quantum efficiency, the absorption gap is 3-cm thick.⁷⁹

Table 10 Technology readiness level—payload—ISODY+ optical assembly.

Subsystem/unit	TRL	Remarks
Telescope	5	ADHE-RP-CGS-001, November 14, 2008, ADAHELI—phase-A report
FPI	6	Off-the-shelf equipment Lidar Tech. Ltd., September 19, 2008, assessment of Fabry–Pérot etalon system for ISODY
CSE controller	4	Off-the-shelf equipment Lidar Tech. Ltd., September 19, 2008, assessment of Fabry–Pérot etalon system for ISODY
Data handling electronics	5	ADHE-RP-CGS-001, November 14, 2008, ADAHELI—phase-A report
Thermal control	5	ADHE-RP-CGS-001, November 14, 2008, ADAHELI—phase-A report

5.2.2 XSPO detector array

XSPO comprises of four photoelectric polarimeters based on the GPD technology. One of them is coupled with a tungsten-coded mask aperture (CMA) needed to localize solar flares on the solar disc with an angular resolution of about 1'. The CMA has a 70' × 70' fully coded FOV (the solar diameter is about 30'). This detector/mask configuration allows exploiting the GPD

Table 11 Technology readiness level—payload—XSPO assembly.

Subsystem/unit	TRL	Remarks
GPD	5	By ESA certification in XPOL polarimeter on board IXO mission. New prototype available in next months
Back end	6	Off-the-shelf equipment IXO-XPOL-MD-006-01, June 28, 2010, IXO—XPOL instrument assessment reports
Control electronics	6	Off-the-shelf equipment IXO-XPOL-MD-006-01, June 28, 2010, IXO—XPOL instrument assessment reports
Thermal control	6	Off-the-shelf equipment IXO-XPOL-MD-006-01, June 28, 2010, IXO—XPOL instrument assessment reports
CMA and FAD	6	Heritage from SuperAGILE experiment on board AGILE satellite
DaMST		
PDHU	9	Unit based on flight proven HW and SW
XBU	9	Unit based on flight proven HW
Antenna	9	Unit based on flight proven HW

imaging capability to localize flares onto the solar disc, but having a minimal impact on the mission profile. The other three GPD units are coupled with simple field angular delimiters (FADs). The solar x-ray flux at energies less than 15 keV is too high for the detector functionality and, moreover, the polarization is expected to be very marginal, therefore a fix multilayer gray filter (as a baseline, 5 μm copper foil + 200 μm titanium + 200 μm aluminum) is foreseen in front of each detector beryllium window to remove low-energy photons which otherwise would completely overwhelm the HXR component. Therefore, the polarimeter configuration chosen is effective in the 15- to 35-keV energy band.

XSPO allows reaching a minimum detectable polarization^{80,81} of 1% for an X5.1 class flare and 5% for an M5.2 class flare. (Spectral data are taken from Ref. 82 by summing the flux from two footpoints since the polarimeter configuration used is not able to separate spatially their emission.)⁸³ During 2 years of mission operation (from 2017 to 2018) about 20 flares are expected to be observed between the X10 and M5 classes, even if the observations will be performed during the decreasing phase of the solar cycle.

The main parameters of XSPO are summarized in Table 8.

6 Technology Readiness, Heritage, and Development Model

ADAHELI+ is based on the heritage of the ADAHELI project, whose phase-A study, awarded in late 2007, had run for 1 year under a 700,000 Euros contract on the ASI Small Missions Program budget. ADAHELI+ benefits from this heritage in terms of satellite subsystems and components, and also from the overall experience and expertise gained by the prime contractor CGS/OHB experience on the successful small mission ASI/AGILE (launched in 2007), in terms of development model, design-to-cost, and a model of team integration between industry and research centers, which proved extremely effective and cost-efficient. After the successful completion of ADAHELI phase-A, the B/C/D phase proposal from industry, universities, and research centers had been submitted to ASI with an overall mission costs of about 50 million Euros. The figures presented hereafter are based on that proposal, taking into account the enhancements and changes proposed for ADAHELI+. All involved technologies have TRL (The TRL standard we refer to in this paper is that employed by ESA at the time of the proposal. The ESA TRL was later revised to conform to the new ISO TRL. For further information refer to Refs. 84 and 85.) higher than 5. Further experience has been gained through the ESA/ARMES activity, an ESA/Startiger program, addressing the fine actuation of the mirrors that will be used for the image stabilization system.

The ISODY+ telescope main structure, designed by SRS Engineering Design, Rome, is composed of 2 hexapods supporting the top ring (with M2 and the heat rejector) and the mirror cell (with M1). The structure candidate material is carbon fiber-reinforced plastic (CFRP), a solution similar to the similarly sized HINODE SOT.

Candidate materials for ISODY+ main mirrors (M1 and M2) are Zerodur or ultralow expansion (ULE) glass. Several configurations have been analyzed in order to find a baseline for the focal plane instruments layout. The selected configuration for the focal plane suite, described previously, is made of reflective elements only: all the objectives located inside the focal plane suite and the collimating unit are conceived as off-axis 2-mirror

telescopes. The small off-axis of the collimating unit introduces negligible polarization, but avoids any vignetting problem caused by the obstruction. A great advantage is the complete independence of the optical system from the wavelength. Each channel (CRTC, BBC, NBC) uses the same optical components as the others: This is very advantageous in terms of cost and accommodation.

The total mass of a CSE-FPI in ISODY+ would be 4.76 kg, including the electronics. The power consumption would be <5 W. While the FPI has been fully environmentally tested for space application, its CSE controller has not been tested yet. It is envisaged to take a terrestrial CSE controller and modify the design to utilize space qualified components and to qualify the CSE controller for space. This information is retrieved from an assessment produced by Lidar Technologies Ltd.

The candidate sensors for the NBC and BBC channels are based on the HAWAII-2RG. The HAWAII-2RG still represents the most advanced imaging sensor technologies for NIR and visible astronomy. Since its introduction, the HAWAII-2RG has been selected for a large number of space- and ground-based instruments, including the James Webb Space Telescope.

The GPD in XSPO derives from the unit developed for the XPOL polarimeter on board the IXO mission, which has been tested in relevant environments (vibrations, thermo-vacuum, and heavy ions) and it is certified as TRL5 by ESA for on board the IXO mission (IXO-XPOL-MD-006-01, June 28, 2010, IXO-XPOL Instrument Assessment Reports). The change of parameters such as the gas mixture, the pressure condition, and the gas absorption depth (for increasing the quantum efficiency at higher energy for solar observations) does not impact on the technology readiness of the instrument. The new prototype with the Ar (60%)–DME (40%) will soon be available for testing. Electronic devices are quoted as TRL6/7 for the XPOL polarimeter on board of IXO (IXO-XPOL-MD-006-01, June 28, 2010, IXO-XPOL Instrument Assessment Reports) since they are based on off-the-shelf equipment. The CMA and the FAD benefit from the heritage of the SuperAGILE experiment, flying on board the ASI/AGILE satellite. It is equipped with a 1-D CMA operating in the energy band 18 to 60 keV⁸⁶ and with a carbon fiber/tungsten field delimiter developed by INAF-Institute for Space Astrophysics and Planetology. Since the GPD is a 2-D pixel detector a 2-D mask pattern needs to be produced for the ADAHELI+ photoelectric polarimeter. In Tables 9–11, a summary of the technology readiness level of the ADAHELI+ platform and payload is reported. The platform makes widespread use of commercial off-the-shelf equipment and, for the elements that require mission dependent customization, only consolidated technologies are considered, therefore the TRL applicable to the platform elements is 9. The development plan and model philosophy are typical of a small mission, with limitations in time and costs, in particular: a protoflight model approach, with engineering models of the critical parts, and early breadboarding of the novel technologies.

7 Mission Profile

Trade-off studies performed over Sun-synchronous circular and elliptical orbits and high elliptical orbits, resulted in the selection of a dawn-dusk, Sun-synchronous, circular orbit at an altitude of 800 km. This orbit allows for continuous sunward pointing and limited eclipses, thus allowing long observing campaigns, while still keeping Doppler shift requirements, set by the tunable

interferometers, within its limits. As a solar observatory, ADAHELI+ typical observations last 24 h, with continuous data acquisition from ISODY+. Data acquisition is switched to the XSPO instrument only during flare events.

The selected orbit⁸⁷ allows for 10 months per year of eclipse-free observations. For the remaining 2 months, the duration of the umbra phase has a peak of about 17 min. Doppler shift is always lower than 4 km/s, and, for over 50% of the time, below 2 km/s. Nominal mission lifetime is 2 years, although spacecraft resources will allow a 1-year extension. In order to minimize the impact of launch costs on the available budget, 2 possible launch options have been considered, matching mass, volume, and cost constraints:

- Shared VEGA launch configuration; as primary payload.
- Single or shared launch configuration with a Polar Satellite Launch Vehicle (PSLV) launcher.

Both launchers are capable of reaching the selected orbit with wide margins in term of mass and their fairing makes possible a lower-cost, shared-launch configuration. Figure 5 shows 2 possible shared-launch accommodations for the ADAHELI+ spacecraft.

8 Operations Concept

ADAHELI+ is a solar observatory for long-duration, high cadence, continuous observations. During data acquisition, the spacecraft operates autonomously without need of intervention from the ground. Several consecutive observation sessions may be stored on the on-board scheduler, allowing a few days of autonomous operations of the space segment. Downloads of payload data are managed through a contact table, containing the ground station visibility periods. These are calculated by the flight dynamic center, based on the satellite attitude defined for the current observation session and are uploaded on board periodically. A similar concept is also applied to the management of the contact with the control station, where the link with the spacecraft is available with any attitude. Observation parameters, such as start time, duration, satellite attitude, etc.,

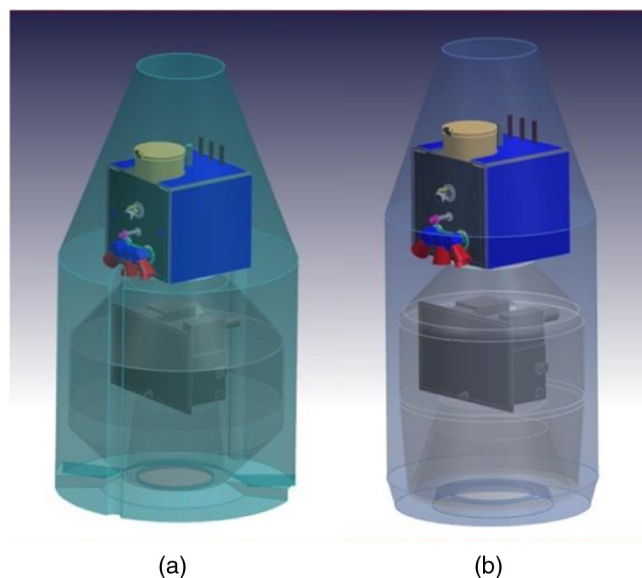


Fig. 5 (a) Polar Satellite Launch Vehicle (PSLV) and (b) Vega accommodations for ADAHELI+ in launch configuration.

are managed through the planning facility on the ground, and are uploaded through a dedicated scheduler. The ground stations are located in the same geographical region. This allows the activities related to spacecraft monitoring and control, and the download of the payload data, to be performed simultaneously. We note that data acquisition may proceed without interruptions during the contacts with the ground stations.

9 Spacecraft Subsystems

The payload and the platform are integrated in the same structure: all the internal units are accommodated around the main telescope of the ISODY+ instrument (see Fig. 6).

9.1 Attitude Control and Pointing Requirements

The requirements on the AOCS to keep the pointing during the telescope's nominal operations are exceptionally stringent for such a class of satellite. In order for the target ROI to fall within the FOV of the high-resolution telescope, the initial accuracy in pointing needs to be a fraction of the FOV that amounts to less than 50 arc sec. The precision in tracking the ROI, then, must be significantly higher, i.e., <0.1 arc sec for the whole duration of the acquisition, in order to meet the required high quality of the image series. Four reaction wheels and a set of three star trackers together with additional sensors (magnetometers and coarse Sun-sensors) and actuators (magnetic torquers) provide a stabilization device within the payload that ensures the required pointing accuracy of 48 arc sec and a pointing knowledge of 25 arc sec. The magnetic torquers also provide the capability to desaturate the wheels and guarantee the survival of the satellite in contingency. The fine tracking of the ROI during acquisition is then implemented through ISODY+ CTCR and TTM (see Sec. 5.1).

9.2 Orbit Control

Orbit control is provided by a hydrazine monopropellant system in order to ensure the maintenance of the target orbit parameters and to perform the deorbiting at the end of the mission. During Nominal Mission, ADAHELI+ Sun-synchronous orbit will enable the telescopes to constantly point the Sun (except during

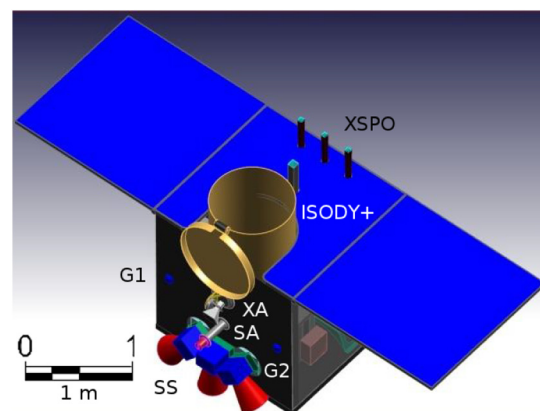


Fig. 6 ADAHELI+ fully deployed layout along with the dimension scale. Some structures are highlighted with different colors: the ISODY+ telescope tube is in yellow-gold; the XSPO field delimiters are in cyan; the S-band (SA) and X-band (XA) antennas are in gray; the GPS (G1 and G2) are in blue; the three star sensors (SS) are in blue and red.

maneuvers, eclipses, or contingencies). The satellite radial velocity in the sunward direction will not exceed ± 4 km/s, during 95% of the Earth orbit around the Sun, thus simplifying the observation schedule upload.

9.3 Platform

The platform architecture is designed to be fully redundant, while the payload uses a modular approach to ensure that a failure of one element causes only a degradation of the overall performances, not the loss of the whole mission. The ADAHELI+ platform uses the platform built by CGS for the ASI/AGILE mission and benefits from the improvements developed for the ASI/PRISMA mission. Communication to the ground is ensured by an S-band transceiver composed of a network of 2 hemispheric antennas. This ensures a link to the ground station with any satellite attitude. Power is generated via a deployable solar array (with a total surface of about 3 m²), and stored using Li-ion rechargeable batteries. The thermal control is passive and is based on dissipation of the internal power through dedicated radiators. In ISODY+, particular care is given to the Sun light entering the telescope and falling on the primary mirror; a dedicated heat rejecter assembly is needed to ensure a drastic reduction of the light heat power reflected from the primary mirror. Spacecraft mass is 510 kg, split between platform (280 kg) and payload (230 kg). Power budget is 450 W.

9.4 Data Downlink

The ADAHELI+ ground segment will comprise of 2 main centers located in Italy: satellite monitoring and control will be orchestrated at Fucino Station (S-band), while payload data acquisition will be taken care of at Matera Station (X-band). The geographical proximity of the 2 ground stations provides almost simultaneous visibility. Considering the selected orbit, the daily visibility is about 50 min, divided in 2 groups of 2 or 3 consecutive passages occurring in early morning and late afternoon (local time). However, the attitude constraints during observations, together with the limited coverage of the high-performance X-band antenna, reduce the available contact time to the ground station for data download. The selected orbit, which has been also designed to maximize the visibility, guarantees a visibility time for payload data download of at least 25 min/day.

The total amount of data generated by the payload is 22 GBytes/day. In order to download the data acquired in 1 day, a data rate in downlink of at least 120 Mbps is required. Taking into account overhead and margins on generated data, the selected transmitter has a data rate of 150 Mbps. Mass memory capacity dedicated to the payload data is constrained by the limited availability of ground station visibility, concentrated around a few orbits per day. Due to the constraint of the limited availability of ground station visibility, the mass memory needed on-board has been estimated to be 24 GBytes.

- Satellite and mission control center, at Fucino (IT), in charge of: mission planning and control. Merging and planning the operations and requests from the G/S context including: checking and harmonization of user requests, generating satellite tasking plan and satellite pointing and control. Orbit management includes: orbit prediction, maneuvers calculation, attitude calculation, and thruster firing prediction and those activities required to track

the TM satellite beacon, to manage the satellite TM and TC.

- Payload ground segment center, at Matera (IT), in charge of mission exploitation activities. Acquiring, archiving, and processing the scientific data transmitted by the satellite and providing support to users, from requests to data delivery.

10 Summary and Conclusions

The ADAHELI+ project is a Small Solar and Space Weather Mission with a budget compatible with an ESA S-class mission, including launch, and a fast development cycle. The mission builds on the phase-A study financed by ASI of the former ADAHELI mission.

The main scientific goals of the ADAHELI+ mission are the study of the coupling of the photosphere, chromosphere, and corona by the magnetic field; the generation and destruction of the magnetic field itself in the solar atmosphere; and the determination of the polarization state of the x-ray emission by flares from the solar atmosphere.

To address these topics, ADAHELI+ has been designed with a novel payload, composed of:

ISODY+: A spectropolarimetric imager, whose design is optimized for high cadence, long-duration, multiline polarimetry in the VIS–NIR region of the solar spectrum.

The feasibility study of ISODY+ optics has been done successfully, by exploring designs based on different concepts, and with a wide overview of the critical points and possible solutions. The tomographic and polarimetric capabilities and fast cadence of ISODY+ will give us a chance to solve the mystery of the solar superhot corona or resolve fundamental problems in solar physics, such as the origin and acceleration of the fast solar wind.

XSPO: An x-ray polarimeter, which will perform sensitive polarimetry of solar flares in the 15 to 35 keV range.

So far, no relevant x-ray polarimetry measure of solar flares has been obtained by past observations and there is still a lack of precise measurements. XSPO on board ADAHELI+ would fill this gap, providing for the first time 2 more observational parameters (polarization angle and degree) to the study of Solar flares.

To allow the most complete exploit of its instrumentation, and at the same time matching the constraints of a limited budget, innovative solutions have been proposed:

- compact design for the VIS–NIR instrument with an all-reflective setup;
- CSE–FPI-based imager fed by a 50-cm Gregorian telescope;
- different observation profiles for high cadence spectrometry, high resolution, and/or high sensitivity spectropolarimetry;
- GPD-based detectors for the measure of the polarization of x-rays;
- continuous and long-duration observations due to available on-board memory and choice of suitable orbit;

- possible shared launch, both with a VEGA and a PSLV launcher.

Through its set of instruments, ADAHELI+ will open a new window to the investigation and understanding of processes in the solar plasma and magnetic fields and will address key questions concerning the physics of the Sun and heliosphere.

Acknowledgments

This paper was dedicated to the memory of Paolo Sabatini, who passed away on July 21, 2015.

References

1. F. Berrilli et al., “The ADAHELI (advanced astronomy for heliophysics) solar mission,” *Mem. Soc. Astron. Ital.* **80**, 251 (2009).
2. F. Berrilli et al., “The ADAHELI solar mission: investigating the structure of sun’s lower atmosphere,” *Adv. Space Res.* **45**, 1191–1202 (2010).
3. V. Greco, F. Cavallini, and F. Berrilli, “The telescope and the double Fabry–Pérot interferometer for the ADAHELI solar space mission,” *Proc. SPIE* **7731**, 773142 (2010).
4. F. Berrilli et al., “The Fabry–Pérot interferometer prototype for the ADAHELI solar small mission,” *Proc. SPIE* **8148**, 814807 (2011).
5. P. F. Moretti et al., “Future instrumentation for solar physics: a double channel MOF imager on board ASI space mission ADAHELI,” *Astrophys. Space Sci.* **328**, 313–318 (2010).
6. M. Stangalini et al., “DIMMI-2h a MOF-based instrument for solar satellite ADAHELI,” *Proc. SPIE* **8148**, 81480U (2011).
7. G. Hernandez, “Fabry–Pérot Interferometers,” *Cambridge Studies in Modern Optic*, P. L. Knight and A. Miller, Eds., Cambridge University Press (1986).
8. R. Doyon et al., “The JWST tunable filter imager (TFI),” *Proc. SPIE* **7010**, 70100X (2008).
9. I. Yoshikawa et al., “The mercury sodium atmospheric spectral imager for the MMO spacecraft of Bepi-Colombo,” *Planet. Space Sci.* **58**, 224–237 (2010).
10. S. K. Solanki et al., “The polarimetric and helioseismic imager for solar orbiter: SO/PHI,” in *Proc. Int. Astronomical Union*, Vol. 305, pp. 108–113 (2015).
11. L. Giovannelli et al., “Testing of the “Tor Vergata” Fabry–Pérot interferometer prototype,” *Proc. SPIE* **8446**, 84463Q (2012).
12. E. Costa et al., “An efficient photoelectric X-ray polarimeter for the study of black holes and neutron stars,” *Nature* **411**, 662–665 (2001).
13. R. Bellazzini et al., “Novel gaseous X-ray polarimeter: data analysis and simulation,” *Proc. SPIE* **4843**, 383–393 (2003).
14. A. Vecchio, G. Cauzzi, and K. P. Reardon, “The solar chromosphere at high resolution with IBIS. II. Acoustic shocks in the quiet internetwork and the role of magnetic fields,” *Astron. Astrophys.* **494**, 269–286 (2009).
15. M. Stangalini et al., “Three-minute wave enhancement in the solar photosphere,” *Astron. Astrophys.* **539**, L4 (2012).
16. M. Stangalini, F. Berrilli, and G. Consolini, “The spectrum of kink-like oscillations of solar photospheric magnetic elements,” *Astron. Astrophys.* **559**, A88 (2013).
17. H. Alfvén, “Magneto hydrodynamic waves, and the heating of the solar corona,” *Mon. Not. R. Astron. Soc.* **107**, 211 (1947).
18. D. Rabin and R. Moore, “Heating the sun’s lower transition region with fine-scale electric currents,” *Astrophys. J.* **285**, 359–367 (1984).
19. E. N. Parker, “Nanoflares and the solar X-ray corona,” *Astrophys. J.* **330**, 474–479 (1988).
20. F. Cattaneo, T. Emonet, and N. Weiss, “On the interaction between convection and magnetic fields,” *Astrophys. J.* **588**, 1183–1198 (2003).
21. J. Sánchez Almeida et al., “Magnetic bright points in the quiet sun,” *Astrophys. J. Lett.* **715**, L26–L29 (2010).
22. J. A. Bonet, I. Cabello, and J. Sánchez Almeida, “Center-to-limb variation of the area covered by magnetic bright points in the quiet sun,” *Astron. Astrophys.* **539**, A6 (2012).
23. S. Jafarzadeh et al., “Structure and dynamics of isolated internetwork Ca II H bright points observed by SUNRISE,” *Astron. Astrophys.* **549**, A116 (2013).
24. D. B. Jess et al., “Multiwavelength studies of MHD waves in the solar chromosphere—an overview of recent results,” *Space Sci. Rev.* **190**, 103–161 (2015).
25. R. J. Morton et al., “The generation and damping of propagating MHD kink waves in the solar atmosphere,” *Astrophys. J.* **784**, 29 (2014).
26. M. Stangalini et al., “Observational evidence for buffeting-induced kink waves in solar magnetic elements,” *Astron. Astrophys.* **569**, A102 (2014).
27. M. Stangalini, F. Giannattasio, and S. Jafarzadeh, “Non-linear propagation of kink waves to the solar chromosphere,” *Astron. Astrophys.* **577**, A17 (2015).
28. J. M. Beckers, “Solar spicules,” *Sol. Phys.* **3**, 367–433 (1968) [Invited Review Paper].
29. L. H. M. R. Van der Voort et al., “Magnetoacoustic shocks as a driver of quiet-sun mottles,” *Astrophys. J. Lett.* **660**, L169–L172 (2007).
30. A. G. de Wijn and B. De Pontieu, “Dynamic fibrils in H α and C IV,” *Astron. Astrophys.* **460**, 309–316 (2006).
31. B. De Pontieu et al., “High-resolution observations and modeling of dynamic fibrils,” *Astrophys. J.* **655**, 624–641 (2007).
32. N. Deng et al., “Chromospheric rapid blueshifted excursions observed with IBIS and their association with photospheric magnetic field evolution,” *Astrophys. J.* **799**, 219 (2015).
33. L. R. van der Voort et al., “On-disk counterparts of type II spicules in the Ca II 854.2 nm and H α lines,” *Astrophys. J.* **705**, 272–284 (2009).
34. D. H. Sekse et al., “Statistical properties of the disk counterparts of type II spicules from simultaneous observations of rapid blueshifted excursions in Ca II 8542 and H α ,” *Astrophys. J.* **752**, 108 (2012).
35. L. Ofman, “Wave modeling of the solar wind,” *Living Rev. Sol. Phys.* **7**, 4 (2010).
36. B. W. Lites et al., “The horizontal magnetic flux of the quiet-sun internetwork as observed with the Hinode spectro-polarimeter,” *Astrophys. J.* **672**, 1237–1253 (2008).
37. R. Ishikawa, S. Tsuneta, and J. Jurčák, “Three-dimensional view of transient horizontal magnetic fields in the photosphere,” *Astrophys. J.* **713**, 1310–1321 (2010).
38. R. Ishikawa and S. Tsuneta, “Spatial and temporal distributions of transient horizontal magnetic fields with deep exposure,” *Astrophys. J. Lett.* **718**, L171–L175 (2010).
39. A. G. de Wijn et al., “Hinode observations of magnetic elements in internetwork areas,” *Astrophys. J.* **684**, 1469–1476 (2008).
40. A. G. de Wijn et al., “Small-scale solar magnetic fields,” *Space Sci. Rev.* **144**, 275–315 (2009).
41. S. Tsuneta et al., “The solar optical telescope for the Hinode mission: an overview,” *Sol. Phys.* **249**, 167–196 (2008).
42. V. Martínez Pillet et al., “The imaging magnetograph experiment (IMaX) for the sunrise balloon-borne solar observatory,” *Sol. Phys.* **268**, 57–102 (2011).
43. S. K. Solanki et al., “SUNRISE: instrument, mission, data, and first results,” *Astrophys. J. Lett.* **723**, L127–L133 (2010).
44. P. Barthol et al., “The sunrise mission,” *Sol. Phys.* **268**, 1–34 (2011).
45. A. Lagg et al., “Fully resolved quiet-sun magnetic flux tube observed with the SUNRISE/IMaX instrument,” *Astrophys. J. Lett.* **723**, L164–L168 (2010).
46. J. A. Bonet et al., “SUNRISE/IMaX observations of convectively driven vortex flows in the sun,” *Astrophys. J. Lett.* **723**, L139–L143 (2010).
47. A. Vögler and M. Schüssler, “A solar surface dynamo,” *Astron. Astrophys.* **465**, L43–L46 (2007).
48. J. C. Brown, “The deduction of energy spectra of non-thermal electrons in flares from the observed dynamic spectra of hard X-ray bursts,” *Sol. Phys.* **18**, 489–502 (1971).
49. H. S. Hudson et al., “X-ray searches for solar axions,” in *4th Hinode Science Meeting: Unsolved Problems and Recent Insights*, Palermo, Italy, L. Bellot Rubio, F. Reale, and M. Carlsson, Eds., Astronomical Society of the Pacific Conf. Series, Vol. 455, pp. 25, Astronomical Society of the Pacific, San Francisco (2012).
50. R. P. Lin and H. S. Hudson, “Non-thermal processes in large solar flares,” *Sol. Phys.* **50**, 153–178 (1976).
51. J. C. Brown, A. N. McClymont, and I. S. McLean, “Interpretation of solar hard X-ray burst polarisation measurements,” *Nature* **247**, 448–449 (1974).
52. S. H. Langer and V. Petrosian, “Impulsive solar X-ray bursts. III—polarization, directivity, and spectrum of the reflected and total

- bremsstrahlung radiation from a beam of electrons directed toward the photosphere,” *Astrophys. J.* **215**, 666–676 (1977).
53. A. G. Emslie and L. Vlahos, “Radiation signatures from a locally energized flaring loop,” *Astrophys. J.* **242**, 359–373 (1980).
 54. J. Leach and V. Petrosian, “The impulsive phase of solar flares. II—characteristics of the hard X-rays,” *Astrophys. J.* **269**, 715–727 (1983).
 55. V. V. Zharkova, J. C. Brown, and D. V. Syriavskii, “Electron beam dynamics and hard X-ray bremsstrahlung polarization in a flaring loop with return current and converging magnetic field,” *Astron. Astrophys.* **304**, 284 (1995).
 56. J. E. Charikov, A. B. Guzman, and I. V. Kudryavtsev, “Hard X-ray emission of solar flares and non-stationary kinetics of electron beams,” *Astron. Astrophys.* **308**, 924–928 (1996).
 57. V. V. Zharkova, A. A. Kuznetsov, and T. V. Siversky, “Diagnostics of energetic electrons with anisotropic distributions in solar flares. I. Hard X-rays bremsstrahlung emission,” *Astron. Astrophys.* **512**, A8 (2010).
 58. A. V. Bogomolov et al., “Hard X-ray radiation from solar flares in the second half of 2001: preliminary results of the SPR-N experiment onboard the CORONAS-F satellite,” *Sol. Syst. Res.* **37**, 112–120 (2003).
 59. I. A. Zhitnik et al., “Polarization, temporal, and spectral parameters of solar flare hard X-rays as measured by the SPR-N instrument onboard the CORONAS-F satellite,” *Sol. Syst. Res.* **40**, 93–103 (2006).
 60. I. A. Zhitnik et al., “Experiment with the SPR-N instrument onboard the CORONAS-F satellite: polarization, temporal, and spectral characteristics of the hard X-ray of the solar flares,” in *Astrophysics and Space Science Library*, V. Kuznetsov, Ed., Astrophysics and Space Science Library, Vol. 400, pp. 129, Springer-Verlag, Berlin Heidelberg (2014).
 61. E. Suarez-Garcia et al., “X-ray polarization of solar flares measured with RHESSI,” *Sol. Phys.* **239**, 149–172 (2006).
 62. E. D. Carlson and T. Li-Sheng, “Pseudoscalar conversion and X-rays from the sun,” *Phys. Lett. B* **365**, 193–201 (1996).
 63. I. G. Hannah et al., “Constraining the hard X-ray properties of the quiet sun with new RHESSI observations,” *Astrophys. J.* **724**, 487–492 (2010).
 64. A. Asensio Ramos, J. Trujillo Bueno, and E. Landi Degl’Innocenti, “Advanced forward modeling and inversion of stokes profiles resulting from the joint action of the Hanle and Zeeman effects,” *Astrophys. J.* **683**, 542–565 (2008).
 65. C. Sasso, A. Lagg, and S. K. Solanki, “Milne–Eddington inversions of the He 10 830 Å Stokes profiles: influence of the Paschen-Back effect,” *Astron. Astrophys.* **456**, 367–371 (2006).
 66. C. Sasso, A. Lagg, and S. K. Solanki, “Multicomponent He I 10 830 Å profiles in an active filament,” *Astron. Astrophys.* **526**, A42 (2011).
 67. J. de la Cruz Rodriguez et al., “Non-local thermodynamic equilibrium inversions from a 3D magnetohydrodynamic chromospheric model,” *Astron. Astrophys.* **543**, A34 (2012).
 68. T. Kosugi et al., “The Hinode (Solar-B) mission: an overview,” *Sol. Phys.* **243**, 3–17 (2007).
 69. B. De Pontieu et al., “The interface region imaging spectrograph (IRIS),” *Sol. Phys.* **289**, 2733–2779 (2014).
 70. V. Hansteen et al., “The unresolved fine structure resolved: IRIS observations of the solar transition region,” *Science* **346**(6207), 1255757 (2014).
 71. J. Brault and H. Neckel, “Spectral atlas of solar absolute disk-averaged and disk-center intensity from 3290 to 12510 Å,” ftp.hs.uni-hamburg.de/pub/outgoing/FTS-atlas (1987).
 72. F. Cavallini, “IBIS: a new post-focus instrument for solar imaging spectroscopy,” *Sol. Phys.* **236**, 415–439 (2006).
 73. B. Viticchié et al., “Imaging spectropolarimetry with IBIS: evolution of bright points in the quiet sun,” *Astrophys. J. Lett.* **700**, L145–L148 (2009).
 74. B. Viticchié et al., “Imaging spectropolarimetry with IBIS. II. On the fine structure of G-band bright features,” *Astrophys. J.* **723**, 787–796 (2010).
 75. P. Sabatini et al., “ADAHELI+: an Italian project for the study of the Sun,” in *Atti dei Convegni Lincei*, Vol. 285, p. 65, Convegno Celebrazione del IV Centenario della Pubblicazione dell’Opuscolo Istoria e Dimostrazioni Intorno alle Macchine Solari, Accademia Nazionale dei Lincei (2014).
 76. L. Pacciani et al., “Sensitivity of a photoelectric X-ray polarimeter for astronomy: the impact of the gas mixture and pressure,” *Proc. SPIE* **4843**, 394–405 (2003).
 77. S. Fabiani et al., “The gas pixel detector as a solar X-ray polarimeter and imager,” *Adv. Space Res.* **49**, 143–149 (2012).
 78. S. Fabiani et al., “X-ray polarimetry towards high energy and solar science,” *J. Phys. Conf. Ser.* **383**, 012013 (2012).
 79. S. Fabiani et al., “Performance of an Ar-DME imaging photoelectric polarimeter,” *Proc. SPIE* **8443**, 84431C (2012).
 80. M. C. Weisskopf, R. F. Elsner, and S. L. O’Dell, “On understanding the figures of merit for detection and measurement of X-ray polarization,” *Proc. SPIE* **7732**, 77320E (2010).
 81. T. E. Strohmayer and T. R. Kallman, “On the statistical analysis of X-ray polarization measurements,” *Astrophys. J.* **773**, 103 (2013).
 82. P. Saint-Hilaire, S. Krucker, and R. P. Lin, “A statistical survey of hard X-ray spectral characteristics of solar flares with two footpoints,” *Sol. Phys.* **250**, 53–73 (2008).
 83. S. Fabiani et al., “A solar flares X-ray polarimeter,” *Mem. Soc. Astron. Ital.* **84**, 422 (2013).
 84. ESA TRL Working Group, “Guidelines for the use of TRLs in ESA programmes,” Technical Report ESSB-HB-E-002, European Space Agency (2013).
 85. Committee ISO/TC 20: Aircraft and space vehicles; Subcommittee SC 14: Space systems and operations, “Space systems—definition of the technology readiness Levels (TRLs) and their criteria of assessment,” Technical Report ISO/FDIS 16290:2013, “Space systems – Definition of the Technology Readiness Levels (TRLs) and their criteria of assessment,” ISO/TC 20/SC 14 (2013).
 86. M. Feroci et al., “Monitoring the hard X-ray sky with SuperAGILE,” *Astron. Astrophys.* **510**, A9 (2010).
 87. F. Curti, G. Russo, and F. Longo, “On the orbit selection of the space solar telescope ADAHELI,” *Adv. Astron. Sci.* **135**, 2227–2246 (2010).

Francesco Berrilli is a professor of solar physics and computer science at the University of Rome “Tor Vergata.” He majored in physics at the University of Rome in experimental astrophysics and star formation in 1983 and received Lincean Academy National membership in 2014. His research interests include ground-based and space instruments, image acquisition systems, space weather, and pattern formation in solar convective plasma. He codirects two master schools in science and technology for space and in science education.

Paolo Soffitta is a primo ricercatore (associate) in the IAPS/INAF. He got his degree “cum laude” and his PhD at La Sapienza Rome University. His expertise on design, development, and conduction of x-ray astronomy missions, and particularly in new detector technologies, derives from the participation to the Beppo-SAX and Agile missions. He won the Bruno Rossi Prize for both those contributions. He is the author/coauthor of more than 150 papers in refereed journals.

Biographies for the other authors are not available.